



Simplify your imaging workflows

**Make research imaging workflows accessible, traceable,
and secure with Athena Software for Core Imaging Facilities.**

Thermo Scientific™ Athena Software is a premium imaging data management platform designed for core imaging facilities that support materials science research.

Athena Software ensures traceability of images, metadata, and experimental workflows through an intuitive and collaborative web interface.

Find out more at thermofisher.com/athena

ThermoFisher
SCIENTIFIC

Bioinspired Underwater Adhesion to Rough Substrates by Cavity Collapse of Cupped Microstructures

Yue Wang and René Hensel*

Underwater or wet adhesion is highly desirable for numerous applications but is counteracted by the liquids in the contact which weaken intermolecular attraction. The problem is exacerbated in conjunction with surface roughness when liquids partially remain in grooves or dimples of the substrate. In the present study, a cupped microstructure with a cavity inspired by suction organs of aquatic animals is proposed. The microstructures (cup radius of 100 μm) are made from polyurethane using two-photon lithography followed by replica molding. Adhesion to rough substrates is emulated experimentally by a micropatterned model substrate with varying channel widths. Pull-off stresses are found to be about 200 kPa, i.e., twice atmospheric pressure. Evaluation of force–displacement curves together with in situ observations reveal the adhesion mechanism, which involves adaptation to surface roughness and an elastic force induced by the collapse of the cavity that holds sealed contact with the substrate during retraction. This new microarchitecture may pave the way for next generation microstructures applicable to real, rough surfaces under wet conditions.

1. Introduction

Temporary adhesion under wet conditions is essential for practical applications such as underwater locomotion,^[1] grip and handling of objects,^[2,3] and medical treatments.^[4] Compared to dry adhesion mediated by van der Waals interactions, liquid films in the contact drastically weaken the contact strength due to reduced intermolecular interactions.^[5–7] Surface roughness further complicates the situation as the area of solid–solid contact is reduced and, in addition, liquids can remain in the grooves and dimples of the surface or cause leakage due to percolation.^[8–10] Robust solutions for this adhesion problem have repeatedly been realized in the biological world.^[11]

In the course of evolution, several aquatic animals such as octopus,^[12–14] clingfish,^[9,15] squid,^[16] and net-winged midge larvae^[17,18] have evolved strategies to temporarily adhere to rough surfaces underwater. These attachment organs consist of a central

cavity, formed by muscles and connective tissue and open toward the substrate, and a ring-shaped disc, which establishes contact with the target substrate. While adhesion is due to a pressure difference caused by muscular action, the detailed mechanism of adhesion,^[12–14,19] and especially to rough surfaces,^[8,15,17,20] is still under debate.


To achieve suction, it is necessary to establish intimate contact between the ring-shaped disc and the substrate to create a seal that allows the formation of a pressure gradient between the water trapped inside the cavity and the surrounding medium. To maintain suction over a period of time, leakage through the seal must be avoided.^[21] An intriguing observation is that the surfaces of such contact discs in nature are not smooth, but rather bear microfeatures, whose function has not yet been fully clarified. For octopus, Kier and

Smith discussed microfeatures from the perspective of enhanced shear resistance, which prevents the disc from contracting when the sucker is pulled off.^[20] Similarly, Kang et al. discovered dense arrays of nanoscopic spine-like fibers located at the suction disc of net-winged midge larvae.^[17,18] The fibers are inwardly oriented, which has been suggested to increase shear strength and resist slipping, especially on rough target surfaces. A competing hypothesis is that the microfeatures allow the water to spread into the contact to distribute the hydrostatic pressure homogeneously across the entire interface, maximizing the contact area when the pressure is reduced.^[14] Furthermore, micropatterning enhances the compliance of the surface, enabling better adaptation to a rough substrate.^[22] Wainwright et al. suggested such a structural softening by nano-filaments to enable better sealing of the suction disc of clingfish.^[8] In contrast to these studies, a recent report by Sandoval et al. demonstrated that a clingfish-inspired suction disk with micropillars at the contact area performed worse than a disc without micropillars.^[15]

Suction organs of octopus, clingfish, squid, and net-winged midge larvae are actuated by several muscles, which together with the connective tissue form a cavity. Muscle contraction deforms the cavity and therefore its volume. When in sealed contact with the target substrate, the muscle-induced contraction of the cavity is not compensated by a change in volume due to incompressibility of water, which creates suction.

To be energy efficient in long-term contacts, Kier and Smith suggest as a source of stored strain energy from elastically deformed tissue building the cavity to sustain suction without maintaining muscle contractions.^[14] Similarly, Tramacere et al.

Dr. Y. Wang, Dr. R. Hensel
INM – Leibniz Institute for New Materials
Campus D2 2, 66123 Saarbrücken, Germany
E-mail: rene.hensel@leibniz-inm.de

 The ORCID identification number(s) for the author(s) of this article can be found under <https://doi.org/10.1002/adfm.202101787>.

© 2021 The Authors. Advanced Functional Materials published by Wiley-VCH GmbH. This is an open access article under the terms of the Creative Commons Attribution-NonCommercial License, which permits use, distribution and reproduction in any medium, provided the original work is properly cited and is not used for commercial purposes.

DOI: 10.1002/adfm.202101787

discussed the characteristic shape of the cavity of octopus that exhibits a so-called protuberance that allows to split the water reservoir captured inside the cavity into two separated portions.^[12,13] Upon relaxation of the muscles, the hydrostatic pressure of the water reservoir contacting the target substrate remains low due to the fact that the upper part of the cavity containing the second reservoir try to relax by the stored strain energy of the deformed cavity. Inspired from that findings, synthetic suckers were mimicked and successfully tested underwater. However, their performance against rough substrates were not reported so far.^[23–25] Therefore, the mechanism of large cavity deformation and its role in adhesion to rough substrates remains unclear.

By mimicking the general concept of suction organs discussed above, we recently introduced synthetic cupped microstructures, which adhered to smooth substrates with remarkable pull-off strengths of about 1 MPa both underwater and under completely dry conditions.^[2,3] However, their adhesion to rough substrates was extremely low. In the present study, we extend our previous design by implementing a cavity, similar to that found in aquatic organism such as the octopus that enables large elastic deformations during attachment. We report underwater adhesion tests to micropatterned substrates with channels of various widths ranging from 1 to 50 μm to emulate surface roughness. Pull-off stresses obtained are compared to cupped microstructures without cavities, as a control.

The adhesion mechanism is discussed on the basis of force-displacement curves and in situ observations of the elastic deformation and the contact area.

2. Experimental Section

2.1. Fabrication of Microstructures and Micropatterned Counter Substrates

Two designs were compared in this study: microstructures which contained an internal cavity and microstructures without cavity, both with a cup radius of 100 μm (Figure 1a,b). The microstructures were made from polyurethane using two-photon lithography followed by a replication process as described in the previous reports.^[2,3] Briefly, master templates were printed by using the two-photon lithography system Photonic Professional GT (Nanoscribe, Eggenstein-Leopoldshafen, Germany). A polydimethylsiloxane Sylgard 184 mold (Dow Corning, Midland, USA) was replicated from the master, which was subsequently replicated in polyurethane PMC780 (Smooth-On, Macungie, PA, USA). Polyurethane was mixed by 2:1 of base to cross-linker and cured at 65 $^{\circ}\text{C}$ for at least 12 h in an oven. Upon demolding, microstructures were used without further modifications. The Young's modulus of the polyurethane was about 10 MPa.

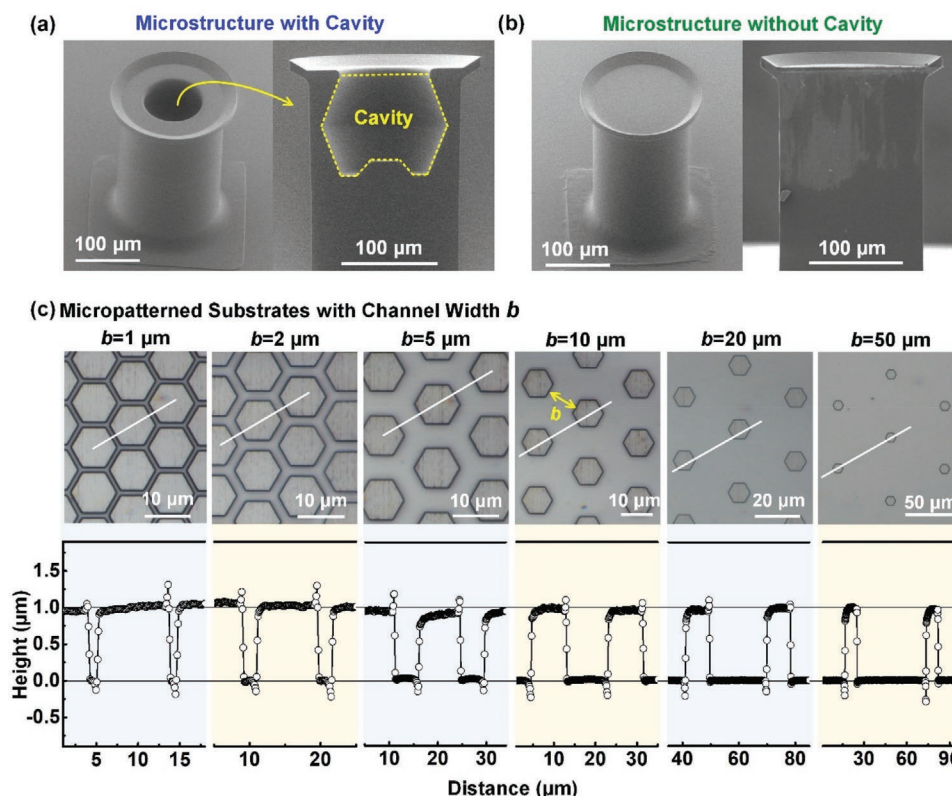


Figure 1. Microstructure and substrate designs. Scanning electron micrographs of cupped polyurethane microstructures a) with and b) without cavity. Left image tilted view; right image cross-section. The dashed line in (a) highlights the cavity. c) Micropatterned substrates to emulate microscopic surface roughness, with hexagons with side length of 5 μm separated by distance, b . White lines indicate the position of the line scans (below). The height of the hexagons was 1 μm for all substrates.

Micropatterned substrates were made in a similar procedure from Epoxy BK (Yachtcare, Uetersen, Germany). First, a template was created by two-photon lithography and then replicated using a PDMS mold. Five parts of the epoxy resin were mixed with three parts of the hardener, cast onto the PDMS mold, and cured at room temperature for 24 h. Cured Epoxy BK had a Young's modulus of 1.8 GPa.^[26] The height profiles of the micropattern were measured using confocal microscopy MarSurf CM explorer (Mahr GmbH, Göttingen, Germany) equipped with a 50× objective.

2.2. Adhesion Measurements

Adhesion tests of individual microstructures were performed using a custom-made device. A 2 N load cell (KD45, ME-Messsysteme, Henningsdorf, Germany) recorded normal forces with a resolution of about 0.3 mN. A piezo-actuated hexapod (SmarPod-110.45.1-s-75, SmarAct GmbH, Oldenburg, Germany) was used to displace the microstructure in vertical direction with 2 nm resolution. In situ observations of side and top views were realized using the Micro Lens System Zoom 640 (Aven, Ann Arbor, MI, USA) attached to a CCD camera DFK 33UX252 (ImagingSource, Bremen, Germany) to record videos.

Before adhesion tests, the microstructure and the micropatterned substrates were submerged in a reservoir of distilled water and degassed at 25 mbar for 10 min. This procedure was necessary to ensure complete wetting without entrapped air bubbles, e.g., inside the cavity. The microstructure was approached to the substrate at a rate of $10 \mu\text{m s}^{-1}$. Compressive preloads were varied between 4 and 24 mN. At preload, the contact was held for 5 s, before the microstructure was retracted at the rate of $10 \mu\text{m s}^{-1}$ until the contact was separated. The maximum tensile force was defined as pull-off force. Nominal pull-off stresses were calculated by dividing the pull-off force values by the projected area of the undeformed cup, i.e., about $3.2 \times 10^4 \mu\text{m}^2$. Each adhesion test was conducted three times.

3. Results and Discussion

The two cupped microstructure designs – with and without a cavity – are depicted in Figure 1a,b. The opening of the cavity faced toward the contact. The cavity was barrel-shaped with a thinner sidewall at the center of the cavity, as highlighted in the cross-section displayed in the right micrograph in Figure 1a. The shape of the cavity was chosen based on the cavities of octopuses.^[12] Nevertheless, the geometry is rather arbitrary and does not correspond to any direct model. The thinner cross-section at the center of the side walls ensures that the cavity bends under compression at this point. All dimensions and the calculation of the cavity volume are summarized in Figure S1 and Table S1 in the Supporting Information. Both microstructure designs had identical stalk diameter and height of 160 and 250 μm , respectively. Cups had an outer diameter of 200 μm and a cup angle of 30°. The micropatterned epoxy substrates are displayed in Figure 1c; protruding hexagons with a side length of 5 μm and a height of 1 μm were arranged hexagonally with distances, b , ranging from 1 to 50 μm (“channel width”).

A schematic of the underwater adhesion tests is shown in Figure 2a. Figure 2b displays pull-off forces obtained for substrate with $b = 10 \mu\text{m}$. Following compressive preloading to low values (<12 mN), the microstructure with cavity showed weak adhesion with pull-off forces below 1 mN. For larger preloads, the pull-off force increased up to 7 mN; this value corresponds to an apparent pull-off stress of 200 kPa. In contrast, the pull-off force of the microstructure without cavity was below 0.5 mN irrespective of the preload.

In order to gain further insight, the force-displacement curves of two set preloads of 8 and 20 mN were examined in more detail (Figure 2c,d). For the microstructure without cavity (Figure 2c), the compressive load increased linearly until preloads of 8 or 20 mN were reached. During retraction, the forces decreased similarly and no adhesion force was measured. For the microstructure with cavity (Figure 2d), the compressive load increased linearly up to an instability at 12 mN, at which the load suddenly dropped by about 1 mN. Subsequently, the compressive load increased again until the preload of 20 mN was reached. During retraction, a hysteresis was observed as the slope of the unloading curve was steeper, suggesting that the contact stiffness had increased upon the instability occurred. An attractive force of 5 mN was subsequently measured. For the set preload of 8 mN, which was below the instability force, the approach and retraction curve formed a small hysteresis, but no adhesion was obtained.

To gain insight into the instability, the elastic deformation (side views) and the contact area (top views) of the microstructure with cavity were analyzed by a series of still images depicted in Figure 3a taken from Videos S1 and S2 (Supporting Information) provided. The water volume entrapped inside the cavity was estimated from side view images (Figure 3c, see Section S1 in the Supporting Information for details). At step A, the microstructure contacted the tops of the hexagons with 10 μm wide channels (compare Figure 3b). In the images taken from the top, dark gray areas represent contact between the microstructure and the substrate, whereas gray refers to non-contact and light gray areas relates to confined water films. During compression, the volume reduced from 1.2×10^6 to $0.9 \times 10^6 \mu\text{m}^3$ with a slope of $5.9 \times 10^6 \mu\text{m}^3 \text{mm}^{-1}$ to step B (Figure 3c). The contact area increased (dark gray circle), but broke at the lower left location, where water suddenly escaped from the cavity. This event was apparently accompanied by a collapse of the cavity and led to the relaxation of the compressive force highlighted in Figure 2d. The cavity volume rapidly decreased down to $\approx 10^5 \mu\text{m}^3$ with a slope of $19.2 \times 10^6 \mu\text{m}^3 \text{mm}^{-1}$. The contact area further increased and resealed, as the microstructure penetrated into the channels between the hexagons until the preload of 20 mN was achieved at step C (Figure 3d). The contact area encompassed several hexagons. It is notable that the cavity had collapsed almost totally and most of the water was squeezed out (volume reduction by one order of magnitude). During retraction, the cavity expanded only slightly to $1.5 \times 10^5 \mu\text{m}^3$ till the compressive force was relaxed to zero (step D). The cavity was still deformed, as water is incompressible and did not invade the cavity through the sealed contact. Once a tensile load was applied, the contact deformed into an elliptical shape and the seal finally broke, at which water suddenly invaded the cavity at step E.

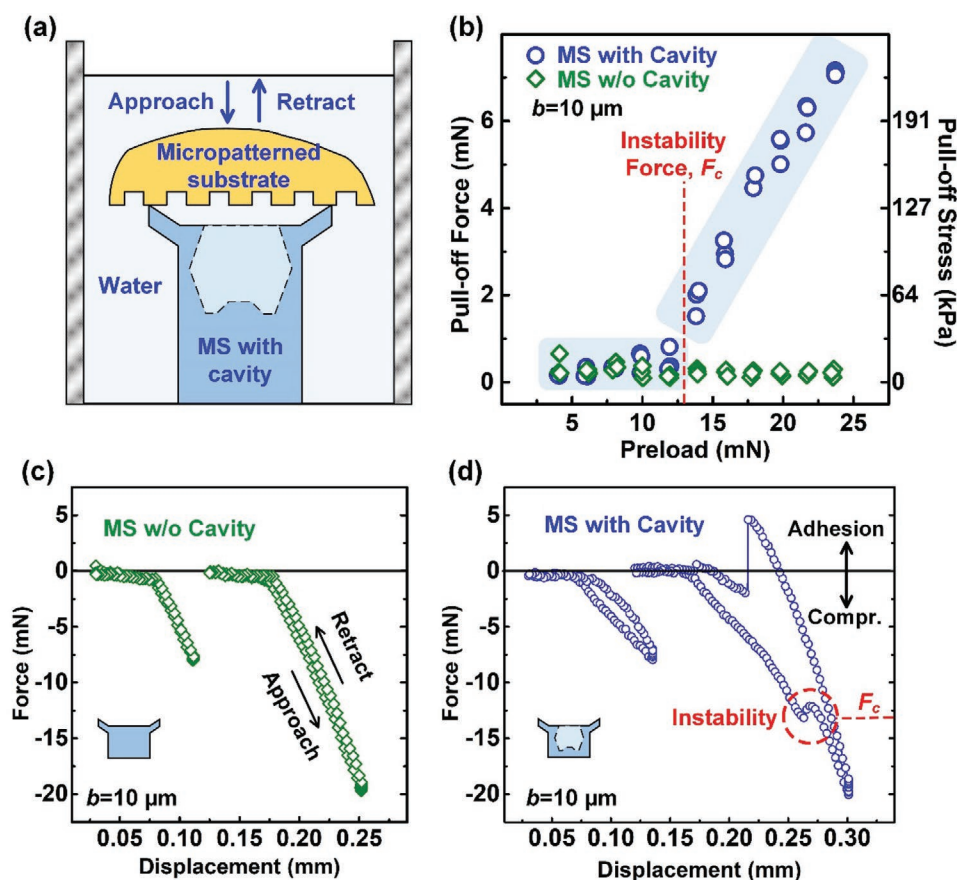


Figure 2. Underwater adhesion test results. a) Illustration of the adhesion test, where the cupped microstructure is immersed in water. b) Pull-off forces and pull-off stresses versus applied compressive preload for three microstructures (MS) with cavity (blue circles) and three MS without cavity (green diamonds). Individual force–displacement curves for 8 and 20 mN preload are shown in c) MS without cavity and d) MS with cavity. The red dashed line in (b) refers to the occurrence of instabilities detected in right force–displacement curve in (d).

Overall, the series of images together with the adhesion results indicate that the compressive force instability is accompanied by a sudden escape of water from the cavity. Two competitive processes take place as the compressive force is increased: the force on the sealing portion of the contact increases while the hydrostatic pressure in the water-filled cavity rises; due to the incompressibility of water, the latter process dominates over the former, eventually giving rise to breakage of the seal.^[27,28] The breakage of the seal corresponds to the instability observed in the force–displacement curves. Simultaneously, the sidewalls of the cavity undergo strong elastic deformation, resulting in additional stored strain energy. The energy maintains a compressive traction that likely keeps contact between the deformed cup and the substrate without leakage when retraction starts. During retraction, the hydrostatic pressure of the remaining water inside the cavity is reduced and creates a suction force, which then enlarges the contact to the substrate. Thus, the suppressed elastic relaxation of the cavity leads to a self-sealing behavior, as depicted in step D in Figure 3a,d and in line with our previous work.^[2,3]

For preloads below the instability force, water did not suddenly escape from the cavity. Figure S2 in the Supporting Information depicts that the cavity volume linearly decreased (approach) and increased (retraction) by $4.9 \times 10^6 \mu\text{m}^3 \text{mm}^{-1}$

for both the approach and the retraction. The result indicates that water was pressed out of the cavity during preloading and vice versa during retraction, most probably via the $10 \mu\text{m}$ wide channels in between the hexagons. However, the volume change together with the elastic deformation of the cavity side walls was not sufficient to store the critical amount of strain energy to initiate the self-sealing mechanism as described above.

To confirm the hypothesis of water flow through the substrate channels, their width, b was varied from 1 to $50 \mu\text{m}$. Figure 4a displays the pull-off force in terms of b and compares it to a smooth substrate with b being infinity. The microstructure with cavity adhered to substrates with $b \geq 10 \mu\text{m}$ with pull-off forces up to about 7 mN depending on the preload. Adhesion to the smooth substrate was similarly high, but insensitive to the preload. For thinner channels ($b < 10 \mu\text{m}$), pull-off forces were below 0.5 mN. High adhesion correlated with the presence of a hysteresis and an instability in the compressive force–displacement curves that were only detected for channels $b \geq 10 \mu\text{m}$ and the smooth substrate (Figure 4c). Instability forces (red circles in Figure 4b) varied between 12.1 mN for $b = 10 \mu\text{m}$ and 6 mN for $b = 50 \mu\text{m}$. The contact images shown in Figure 4d suggest that high adhesion required sealing of the contact area during compression;

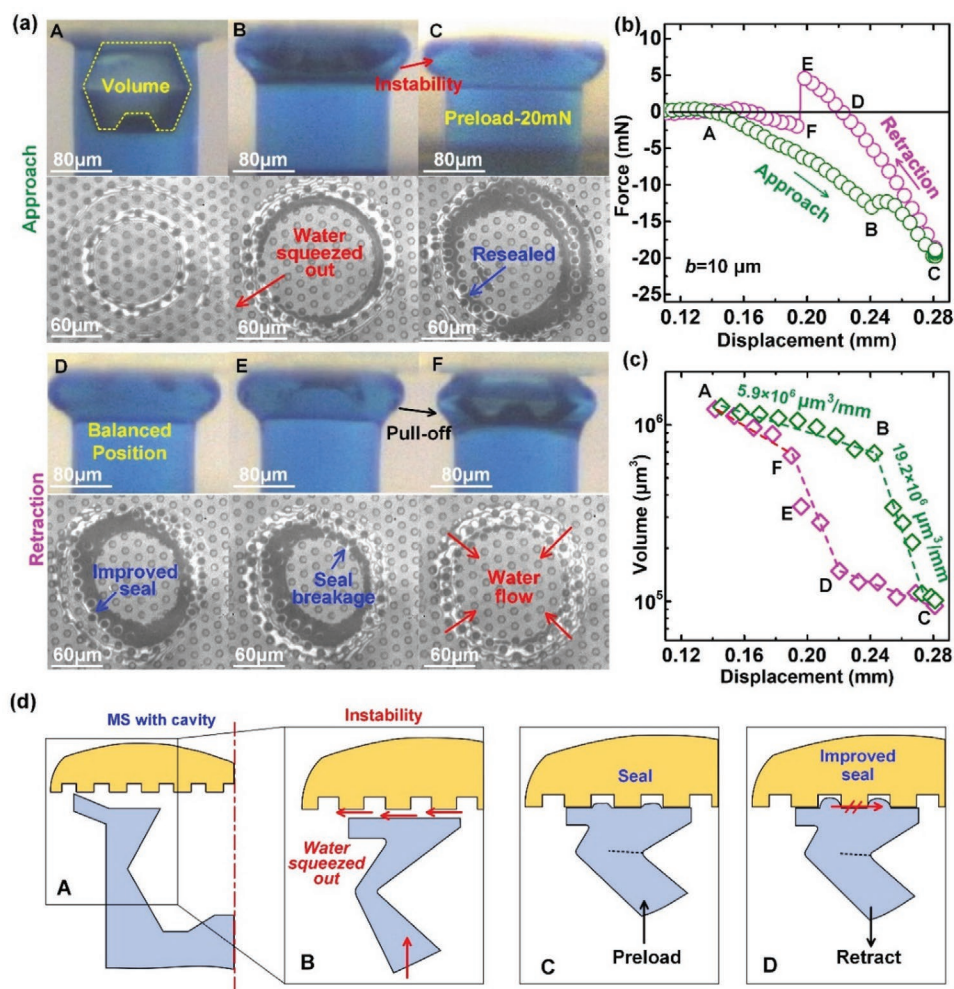


Figure 3. In situ observation of the elastic deformation, instability and contact area. a) Still images from side (upper row, Video S1: Supporting Information) and top (lower row, Video S2: Supporting Information) of the microstructure with cavity during approach (steps A–C) and retraction (steps D–F). b) The corresponding load-displacement curve. c) Change of cavity volume versus displacement. The dashed lines represent linear approximations in each regime. d) Schematic the microstructure with cavity in contact with the micropatterned substrate in steps A, B, C, and D.

this sealing occurred only for $b \geq 10 \mu\text{m}$ and only in the microstructures with a cavity.

The microstructure without cavity adhered weakly with pull-off forces below 2 mN to all substrates (Figure 4b). The only exception was the smooth substrate, where the cupped microstructures adhered strongly with pull-off forces between 20 and 25 mN, which is in agreement with our previous reports.^[2,3] For the rough substrates, the cup section did not adapt to the substrate although the stalk elastically penetrated into the channels irrespective to the channel width, as depicted in the lower row of Figure 4d. Even for large b , the cup section could not adapt to the surface without defects, which impeded sealing. This finding is likely related to the much larger compliance of the cup area than the stalk.

The result demonstrates that only microstructures with cavities enabled underwater adhesion to the micropatterned substrates. To form a seal, leakage through the micropatterned substrate must be avoided. Therefore, the microstructure must elastically deform until it reaches point β at the bottom of the substrate between the channels (compare inset

in Figure 5). Leakage then interrupts, as remaining water is entrapped around the hexagons without percolation. Analytically, the critical compressive stress to attain β can be estimated by Johnson's model of a rigid cylinder indenting an elastic half-space.^[29] The displacement field, $u(x)$ gives the surface profile of the deformed elastic upon indentation as follows:

$$u(x) = \delta_z - \frac{2F}{\pi E^*} \ln \left\{ \frac{x}{a} + \sqrt{\frac{x^2}{a^2} - 1} \right\} \quad (1)$$

where x is the lateral distance from the center of the cylinder with radius a , F the applied compressive force, E^* the reduced elastic modulus, δ_z the indentation depth. In our study, $a = 5 \mu\text{m}$ and $\delta_z = 1 \mu\text{m}$, as the equivalent radius of the cylinder equals the side length and the indentation depth equals the height of the hexagons forming the micropatterned substrate, respectively. Boundary conditions are $u(x = a) = \delta_z$ at the edge of the cylinder and $u(x = a + b/2) = 0$

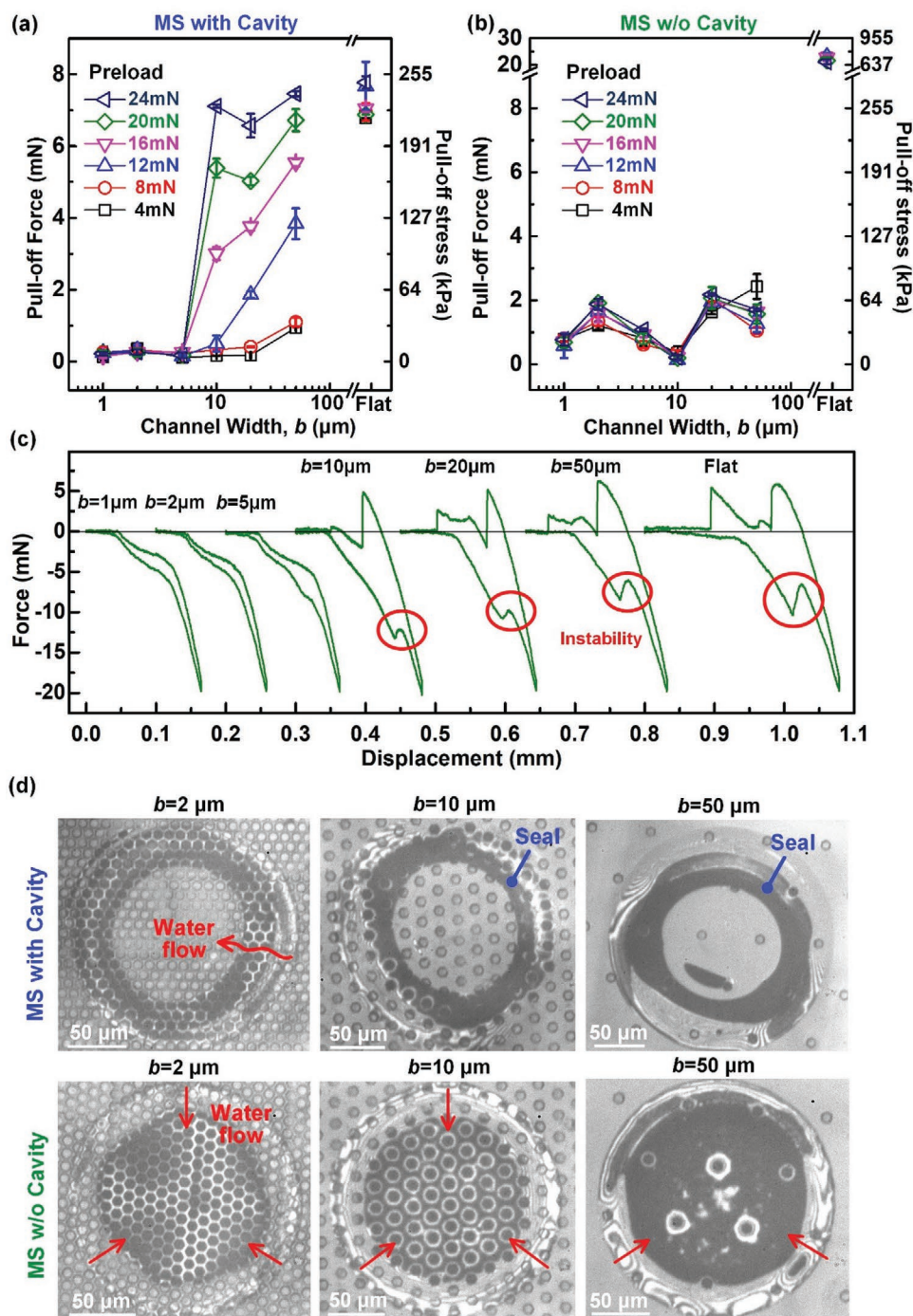


Figure 4. Effect of the channel width, b . Pull-off forces and pull-off stresses in terms of b for the microstructure (MS) a) with and b) without cavity. Various symbols correspond to different preloads. c) Load-displacement curves of the microstructure with cavity adhering to micropatterned substrates with various b . d) The contact area was imaged shortly after retraction was started. Red arrows indicate the direction of water flow during retraction.

at point β . Therefore, the critical force to reach point β , Equation (1) is given by

$$F_c^\beta = \frac{\pi \delta_z E^*}{2 \ln \left\{ 1 + \frac{b}{2a} + \sqrt{\frac{ab + b^2/4}{a^2}} \right\}}$$

The critical force is further divided by the area, πa^2 to obtain the critical stress

$$P_c^\beta = \frac{\delta_z E^*}{\ln \left\{ 1 + \frac{b}{2a} + \sqrt{\frac{ab + b^2/4}{a^2}} \right\} a^2} \quad (2) \quad (3)$$

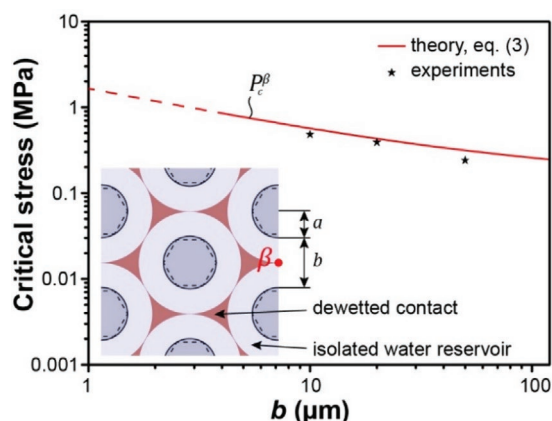


Figure 5. Critical stress versus channel width, b for interrupting leakage through the micropatterned substrate that consist of microcylinders with radius a . Black stars represent the stresses at instability from the experiments shown in Figure 4c. The solid red line corresponds to the theoretical stress to reach point β (Equation (3)) for $\delta_z = 1 \mu\text{m}$, $a = 5 \mu\text{m}$, and $E^* = 13.3 \text{ MPa}$. The dashed line marks where $b \gg \delta_z$ is not satisfied. The inset illustrates the moment when the microstructures touches the bottom of the substrate at point β . Water is then separated into isolated reservoirs (blue) by dewetted contacts (brown) in between.

Note that the critical stress does not account for indentations of an array of hexagons, as elastic coupling of adjacent indents is ignored in the model, which requires $b \gg \delta_z$. Figure 5 displays the results of the analytical model that agree reasonably well with instability stresses obtained from experiments with $b \geq 10 \mu\text{m}$ (Figure 4c); they were calculated as the forces at instability divided by the real contact area of $2.5 \times 10^4 \mu\text{m}^2$ ignoring the cavity. As an example, the predicted compressive stress was about 0.4 MPa to contact the bottom surface between hexagons with $b = 10 \mu\text{m}$, which is close to the instability stress of 0.5 MPa recorded in the experiments. As a general trend, the critical compressive stress that closes the gap between adjacent hexagons increases with decreasing b . Discrepancies between the experiments and theoretical values are most likely associated with the assumption of an elastic half-space in the model instead of finite dimensions of the microstructure.

Overall, to create adhesion to rough substrates via suction, sealing with sufficiently low leakage is required. This is likely achieved by the strain energy stored in the collapsed cavity, which induces sufficient compressive traction to maintain the seal during retraction. Once the hydrostatic pressure of the trapped water inside the cavity decreases, a self-amplifying mechanism engages further sealing during retraction.^[2,3] The importance of the collapsed cavity identified in our experiments likely explains the existence of cavities in natural suction organs. Initiation of suction probably differs between actively muscle-controlled organs and passive microstructures used in our study which were activated by compression. However, our findings clarify that a compressive traction of the cup to the substrate must be maintained during loading to achieve sealing and thus adhesion to rough substrates, which guides toward novel suction gripper designs for improved underwater adhesion to rough substrates.

Figure 6a shows the result of a durability test carried out through 100 cycles of attachment and detachment. Although pull-off forces varied by 20%, it demonstrates repeated adhesion to a rough substrate, rendering the microstructure suitable for applications such as pick-and-place handling or underwater robotics. To generate larger adhesive forces, an array of 9 microstructures was designed and successfully tested, as shown in Figure 6b.

4. Conclusions

Taken together, our study demonstrates that a cavity introduced into the design of cupped microstructures enhances significantly underwater adhesion to rough substrates. The following conclusions can be drawn:

- Microstructures with cavities adhered to micropatterned substrates with $10 \mu\text{m}$ or wider channels. To achieve adhesion, the microstructures must be compressed until an instability is observed, which is accompanied by the release of water from the elastically collapsed cavity.
- Pull-off forces increased with preloads above the critical instability force up to maximum of about 7 mN, which corresponds to a pull-off stress of about 200 kPa.

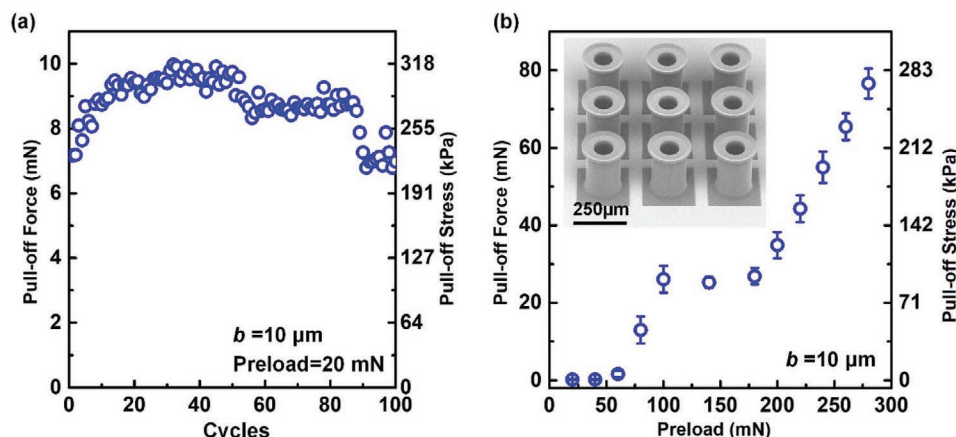


Figure 6. Demonstration of underwater adhesion. a) Pull-off force versus number of cycles demonstrating the durability of a cupped microstructure with cavity against a rough surface with $b = 10 \mu\text{m}$. b) The preload was 20 mN for each cycle.

- c) Microstructures without cavities adhered only very weakly because of the lack of a seal in the cup section, which is essential for creating a suction force.
- d) To further optimize adhesion, the cap of the microstructure should be sufficiently compliant to adapt to surface roughness and diminish leakage, and the stored strain energy in the collapsed cavity should be sufficiently high to keep contact during retraction to induce the self-sealing mechanism. Furthermore, adding microfeatures at the surface of the microstructure may improve the seal formation and the shear resistance, but likely play a minor in creating adhesion to a rough substrate compared to the presence of a cavity.
- e) Admittedly, the regular hexagons on the substrate are a crude approximation of surface roughness. As the height of the channels was kept constant, a constant mean peak-to-valley roughness was modeled by the experiment. The microstructures adapted better to wider channels, which can be considered as long-wavelength roughness. For more realistic topographies, leakage could be computed numerically by several approaches.^[30–34]

Supporting Information

Supporting Information is available from the Wiley Online Library or from the author.

Acknowledgements

The authors gratefully acknowledge fruitful discussions with Prof. Eduard Arzt and acknowledge partial funding by the Leibniz Competition Grant MUSIGAND (No. K279/2019).

Open access funding enabled and organized by Projekt DEAL.

Conflict of Interest

The authors declare no conflict of interest.

Data Availability Statement

Research data are not shared.

Keywords

cavity collapse, cupped microstructures, rough substrates, suction, underwater adhesion

Received: March 8, 2021

Revised: April 21, 2021

Published online:

- [2] Y. Wang, V. Kang, E. Arzt, W. Federle, R. Hensel, *ACS Appl. Mater. Interfaces* **2019**, *11*, 26483.
- [3] Y. Wang, V. Kang, W. Federle, E. Arzt, R. Hensel, *Adv. Mater. Interfaces* **2020**, *7*, 2001269.
- [4] J. J. Green, J. H. Elisseeff, *Nature* **2016**, *540*, 386.
- [5] L. Heepe, A. E. Kovalev, S. N. Gorb, *Beilstein J. Nanotechnol.* **2014**, *5*, 903.
- [6] A. Y. Stark, I. Badge, N. A. Wucinich, T. W. Sullivan, P. H. Niewiarowski, A. Dhinojwala, *Proc. Natl. Acad. Sci. USA* **2013**, *110*, 6340.
- [7] J. Israelachvili, *Intermolecular and Surface Forces*, Elsevier, New York **2011**.
- [8] D. K. Wainwright, T. Kleinteich, A. Kleinteich, S. N. Gorb, A. P. Summers, *Biol. Lett.* **2013**, *9*, 20130234.
- [9] Y.-C. Chuang, H.-K. Chang, G.-L. Liu, P.-Y. Chen, *J. Mech. Behav. Biomed. Mater.* **2017**, *73*, 76.
- [10] M. Chudak, V. Chopra, R. Hensel, A. A. A. Darhuber, *Langmuir* **2020**, *36*, 11929.
- [11] E. Arzt, H. Quan, R. M. McMeeking, R. Hensel, *Prog. Mater. Sci.* **2021**, *119*, 100778.
- [12] F. Tramacere, L. Beccai, M. Kuba, A. Gozzi, A. Bifone, B. Mazzolai, *PLoS One* **2013**, *8*, 65074.
- [13] F. Tramacere, N. M. Pugno, M. J. Kuba, B. Mazzolai, *Interface Focus* **2015**, *5*, 20140050.
- [14] W. M. Kier, *Integr. Comp. Biol.* **2002**, *42*, 1146.
- [15] J. A. Sandoval, S. Jadhav, H. Quan, D. D. Deheyn, M. T. Tolley, *Bioinspir. Biomim.* **2019**, *14*, 066016.
- [16] A. M. Smith, S. M. LaValva, M. M. Loiacono, J. T. Thompson, *J. Exp. Biol.* **2020**, *223*, jeb211227.
- [17] V. Kang, R. Johnston, T. van de Kamp, T. Faragó, W. Federle, *BMC Zool.* **2019**, *4*, 10.
- [18] V. Kang, R. Johnston, T. van de Kamp, T. Faragó, W. Federle, *bioRxiv* **2019**, 666537.
- [19] A. M. Smith, *J. Exp. Biol.* **1991**, *157*, 257.
- [20] W. M. Kier, A. M. Smith, *Biol. Bull.* **1990**, *178*, 126.
- [21] A. Tiwari, B. N. J. Persson, *Soft Matter* **2019**, *15*, 9482.
- [22] V. Barreau, R. Hensel, N. K. Guimard, A. Ghatak, R. M. McMeeking, E. Arzt, *Adv. Funct. Mater.* **2016**, *26*, 4687.
- [23] S. Sareh, K. Althoefer, M. Li, Y. Noh, F. Tramacere, P. Sareh, B. Mazzolai, M. Kovac, *J. R. Soc., Interface* **2017**, *14*, 20170395.
- [24] G. Meloni, O. Tricinci, A. Degl'Innocenti, B. Mazzolai, *Sci. Rep.* **2020**, *10*, 15480.
- [25] B. Mazzolai, A. Mondini, F. Tramacere, G. Riccomi, A. Sadeghi, G. Giordano, E. Del Dottore, M. Scaccia, M. Zampato, S. Carminati, *Adv. Intell. Syst.* **2019**, *1*, 1900041.
- [26] M. Samri, A. Kossa, R. Hensel, *J. Appl. Mech.* **2021**, *88*, 031009.
- [27] B. Lorenz, B. N. J. Persson, *Eur. Phys. J. E* **2010**, *31*, 159.
- [28] B. Lorenz, B. N. J. Persson, *Eur. Phys. J. E* **2010**, *32*, 281.
- [29] K. L. Johnson, *Contact Mechanics*, Cambridge University Press, Cambridge **1985**.
- [30] V. A. Yastrebov, G. Anciaux, J.-F. Molinari, *Tribol. Lett.* **2014**, *56*, 171.
- [31] W. B. Dapp, A. Lücke, B. N. J. Persson, M. H. Müser, *Phys. Rev. Lett.* **2012**, *108*, 244301.
- [32] B. N. J. Persson, N. Prodanov, B. A. Krick, N. Rodriguez, N. Mulakaluri, W. G. Sawyer, P. Mangiagalli, *Eur. Phys. J. E* **2012**, *35*, 5.
- [33] F. Bottiglione, G. Carbone, L. Mangialardi, G. Mantriota, *J. Appl. Phys.* **2009**, *106*, 104902.
- [34] W. B. Dapp, M. H. Müser, *Sci. Rep.* **2016**, *6*, 19513.

[1] Y. Ma, S. Ma, Y. Wu, X. Pei, S. N. Gorb, Z. Wang, W. Liu, F. Zhou, *Adv. Mater.* **2018**, *30*, 1801595.